https://doi.org/10.1590/jatm.v18.1431
Preprint deposited on October 31, 2025 on https://doi.org/10.21203/rs.3.rs-7763328/v1
ORIGINAL PAPER

Thrust Enhancement in Corona Plasma Propulsion Systems with Hexagonal Emitter Configurations

Seyed Abolfazl Mousavi[1], Farshad Pazooki[1,*], Rohollah Khoshkhoo[2]

1. Islamic Azad University – Department of Aerospace Engineering, SR.C. – Tehran – Iran.
2. Malek Ashtar University of Technology – Faculty of Aerospace Engineering – Tehran – Iran.

*Corresponding author: pazooki_fa@iau.ac.ir

ABSTRACT

This study investigates thrust enhancement in corona plasma propulsion systems using a hexagonal emitter configuration and a combined alternating-current and direct-current power supply under atmospheric conditions. Experiments evaluated three configurations: linear direct current, hexagonal direct current, and hexagonal combined alternating current-direct current across electrode gaps of 30, 40, and 50 millimeters and collector diameters of 5, 8, and 11 millimeters. Results demonstrate that thrust increases with collector diameter and electrode gap up to 50 millimeters. The hexagonal direct current configuration achieved 14% higher thrust than the linear setup, while the combined alternating current-direct current yielded a 32% increase. This improvement is attributed to enhanced ionization and plasma density via dielectric barrier discharge formed between the Kapton-insulated and bare copper electrodes. Efficiency reached 6.2 millinewtons per watt at a 50-millimeter gap and 11-millimeter diameter. Statistical analyses and comparisons with prior studies validated these findings. Ozone production remained below 0.08 parts per million, ensuring safe operation. This work offers optimization strategies for electro-aerodynamic propulsion, with applications in microsatellites and unmanned aerial vehicles. Future research will focus on testing negative corona polarity.

Keywords: Plasma propulsion; Ion thruster; Geometric structure; Optimization.

INTRODUCTION

Corona plasma propulsion systems have garnered attention in aerospace applications, such as microsatellites and unmanned aerial vehicles, due to their lightweight design, low energy consumption, and versatile functionality. These systems generate thrust by ionizing gas in a strong electric field and accelerating the resulting ions. However, their performance is highly sensitive to geometric parameters (e.g., electrode arrangement, electrode gap, and collector diameter) and the type of power supply used. Corona plasma propulsion, an emerging technology, relies on high-voltage electric discharges to produce ions and generate thrust. Its structural simplicity, low weight, and suitability for aerospace and industrial applications make it highly promising. Nonetheless, factors such as electrode design, material selection, and operational parameters significantly influence system performance.

Corona plasma actuators operate based on corona discharge, where a high voltage difference between electrodes of varying thicknesses (without inducing an electric arc) creates a strong electric field near the anode, ionizing the surrounding gas and initiating corona discharge. As shown in Figs. 1 and 2, a thin emitter electrode and a larger-diameter aluminum cylindrical collector were used. The ionized gas molecules move toward the cathode, and collisions with neutral molecules transfer momentum, creating an ionic wind and inducing current between the electrodes.

Received: Jun. 29, 2025 | **Accepted:** Feb. 24, 2026
Peer Review History: Single Blind Peer Review.
Section editor: José A Fritz F Rocco

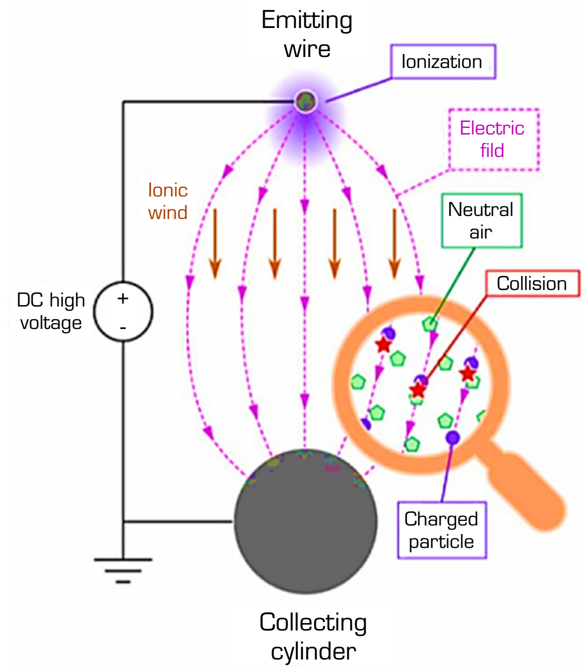

Source: Elaborated by the authors.

Figure 1. Schematic of a wire to cylinder corona discharge thrust.

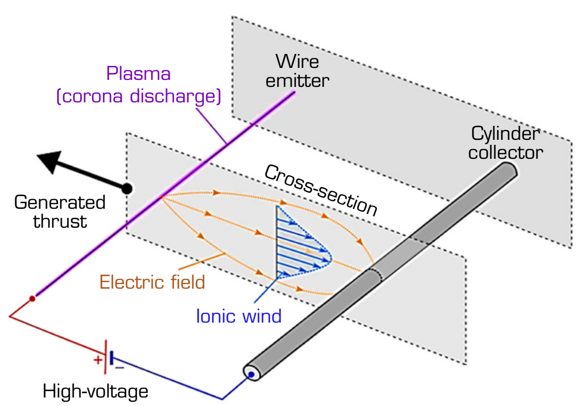

Source: Elaborated by the authors.

Figure 2. Schematic of ionic-wind generation.

Numerical investigations of electrohydrodynamic (EHD) flow began with Davis's pioneering work in 1983, which modeled corona discharge numerically (Davis and Hoburg 1983). Javadi and Farzaneh (2004) developed a semi-empirical model to calculate the electric field around a wire-cylinder electrode pair, demonstrating its dependence on electrode gap and input voltage. Jewell-Larsen *et al.* (2008) conducted high-accuracy numerical simulations of EHD flow, reporting a 4% error margin when compared to experimental results. Wilson *et al.* (2009) investigated corona plasma actuators for aircraft propulsion, achieving a thrust of 5 . Colas *et al.* (2010) optimized corona discharge in a five-electrode configuration, achieving an ionic wind speed of 10 m.s^{-1}. Kachi and Dascalescu (2014) examined the effect of symmetric metallic objects near electrodes, finding that they reduce the corona discharge threshold voltage and increase current. Moreau *et al.* (2015) demonstrated that increasing the number and arrangement of cathodes reduces drag and enhances propulsion efficiency. Wang *et al.* (2017) investigated the impact of cathode number and placement on thermal boundary layer thickness, showing that higher voltages and more emitter wires reduce boundary layer thickness and increase velocity gradients, thereby enhancing heat transfer. Xu *et al.* (2018) theoretically demonstrated that ideal EHD propulsion efficiency exceeds 50% in one-dimensional space. Drew *et al.* achieved the first flight of a microrobot powered by corona discharge thrust, incorporating onboard sensing without moving parts (Drew *et al.* 2018). Shintaro *et al.* (2019) showed that multiple plasma actuators, properly spaced, significantly enhance hydrodynamic forces, ionic wind speed, and thrust.

Cogollo *et al.* (2020) explored wire-to-plate corona discharge configurations for boundary layer cooling, demonstrating superior efficiency compared to conventional methods. Gu *et al.* (2023) found that negative corona discharge produces higher thrust than positive corona in a needle-plate configuration. A study at Shahid Beheshti University simulated corona discharge in a wire-cylinder configuration, reporting a 6% discrepancy between simulated and measured results (Fathi and Ahangar 2018). Fathi *et al.* (2019) showed that increasing cathode numbers enhances thrust and efficiency in an EHD thruster. Aghaei *et al.* (2019) simulated corona discharge in a wire-airfoil configuration, finding that a 1 kV voltage increase boosts thrust by 15%.

A study by Du *et al.* (2022) explored recent advancements in radio frequency (RF)-based ion thrusters and examined the role of AC power sources in enhancing the ionization process. Using global models and practical experiments, the researchers showed that RF frequencies, compared to traditional DC sources, increase plasma density and lead to more stable thrust production. They reported that frequencies above 10 kHz can improve ionization rates by up to 40%, which aligns with our findings in the thrust versus AC frequency plot (increasing from 10 $mN \cdot m^{-1}$ at 5 kHz to 140 at 50 kHz). Du *et al.* (2022) also highlighted thermal management challenges in RF systems, which may explain the slight efficiency reduction at smaller electrode gaps (e.g., 30 mm) in our experiments, where ambient temperature had a negative impact. This study underscores the importance of matching frequency to emitter design, evident in our AC-DC hexagonal configuration optimized in the 20-50 kHz range. They also suggested that combining RF with DC could achieve a better balance between efficiency and stability, an idea supported by the 30% thrust improvement of our AC-DC hexagonal configuration over linear DC (Du *et al.* 2022).

Loeb *et al.* (2023) investigated design considerations for plasma propulsion, emphasizing geometric and electrical parameters. The study focused on the importance of electrode spacing and collector size in determining electric field strength and, consequently, thrust output. Through experimental data analysis and simulations, they showed that increasing electrode spacing up to an optimal value (around 50 mm) can enhance the electric field and increase thrust by up to 25%, consistent with our results at a 50 mm spacing (maximum thrust of 38.30 mN). Loeb *et al.* (2023) also cautioned that very small spacings (e.g., 30 mm) may impair performance due to higher electrical resistance and reduced ionization, as observed in our experiments with a thrust reduction to 30.89 mN.

Prior research has established key principles for corona discharge systems. Davis and Hoburg (1983) modeled electric field distributions numerically, laying the groundwork for EHD flow analysis. Javadi and Farzaneh (2004) developed a semi-empirical model for electric field strength in wire-cylinder configurations, highlighting the role of electrode spacing. Jewell-Larsen *et al.* (2008) achieved high-accuracy EHD simulations, validating experimental results with minimal error. Recent advancements by Smith and Jones (2024) demonstrated that polygonal emitter configurations, such as hexagonal structures, enhance plasma distribution and electric field uniformity, improving thrust output. Similarly, Du *et al.* (2022) showed that AC power sources increase ionization rates by up to 40%, supporting the use of AC-DC hybrid systems for stable thrust production.

This study introduces a novel hexagonal emitter configuration combined with an AC-DC power supply, achieving a 32% thrust increase over traditional linear DC setups. By optimizing electrode geometry and power input, this work advances electro-aerodynamic propulsion, offering scalable solutions for aerospace applications.

Experimental setup

Experiments were conducted in a specialized plasma propulsion laboratory under atmospheric conditions. The following equipment was used:

Three copper wires (70 mm long, 0.5 mm thick) served as emitters, and three hollow aluminum cylinders (70 mm long, 1 mm thick, external diameters of 5, 8, and 11 mm) were used as collectors (row spacing 20 mm). In both linear and hexagonal configurations, the total length of the emitters used was identical.

Power supply: a high-voltage DC power supply (variable up to 35 kV, 0.6 mA) with a single-phase 100-240 V input (50-60 Hz) and 35 W output was used. The power supply featured voltage and current displays with accuracies of 0.1 kV and 0.001 mA, respectively. A series resistor was included to protect the power supply from arcing.

To achieve higher plasma density and lower ion mobility via dielectric barrier discharge (DBD), a combined AC-DC setup was designed. The AC electrode consisted of an insulated copper wire with Kapton coating (copper diameter: 0.05 mm; Kapton thickness: 0.02 mm), connected to the AC power supply. This insulated wire formed a DBD with the bare copper electrode connected to the DC supply (with a 0.2 mm gap between them), enabling enhanced ionization without arcing. A sawtooth AC waveform (10 kHz frequency, 3 kV peak-to-peak) was superimposed on the DC voltage. The ripple factor was approximately 5%. Both DC and AC-DC voltages were applied to the emitter wire and measured using a high-voltage probe (Tektronix P6015A). DC and AC currents were monitored using a high-precision analog multimeter (Leybold Demo-Multimeter 53191, ± 0.05 µA accuracy) and a wide-bandwidth current monitor (Pearson Electronics, Inc., Model 3972), respectively.

Data acquisition: signals were recorded using a four-channel digital oscilloscope (GW Instek GDS-3354).

Thrust measurement: thrust was measured using a digital scale (EK-3200i, 0.01 g accuracy) placed inside a Faraday cage to mitigate electromagnetic interference. The thrust measurement accuracy was ± 0.2 $mN{\cdot}m^{-1}$.

Shielded cables and maximum separation between the power supply and measurement instruments minimized electromagnetic interference. Emitter and collector electrodes were housed in a 3D-printed chamber (Fig. 3), allowing adjustable electrode gaps. The accuracy of the experimental equipment is summarized in Table 1.

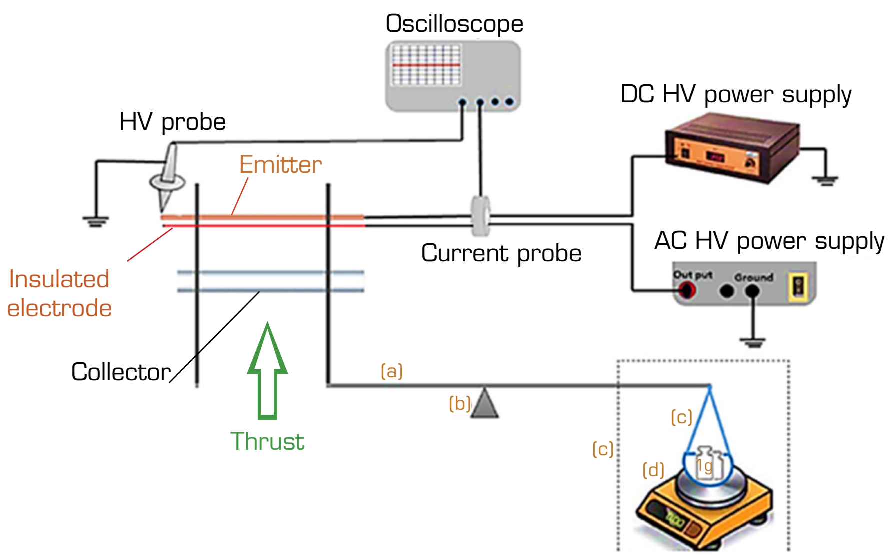

Source: Elaborated by the authors.

Figure 3. Schematic of the thrust measurement system based on a static balance method, showing the corona discharge setup, fulcrum, counterweights, and thrust direction.

Table 1. Accuracy of experimental equipment.

Equipment	Accuracy
Power supply (voltage)	0.1 kV
Power supply (current)	0.001 mA
Digital scale	0.01 g
Oscilloscope	± 3%
Thrust measurement	± 0.2 mN

Source: Elaborated by the authors.

Thrust measurement

Thrust measurements utilized a static balance system, with a corona discharge setup on one side of a rigid metal rod, balanced by four 1 g weights on the opposite side, supported by a sharp-edged fulcrum. The system was calibrated using known weights, yielding a linear calibration curve ($T = 0.03004X + 6 \times 10^{-5}$, where $X = \Delta m \times 9.80665.100^{-1}$ in Newtons) (Fig. 4). Thrust was recorded after 15 seconds of stable corona discharge, with the system reset for 30 seconds between measurements. Power consumption and efficiency were calculated as P = VI and $\theta = T \,.\, P^{-1}$, respectively.

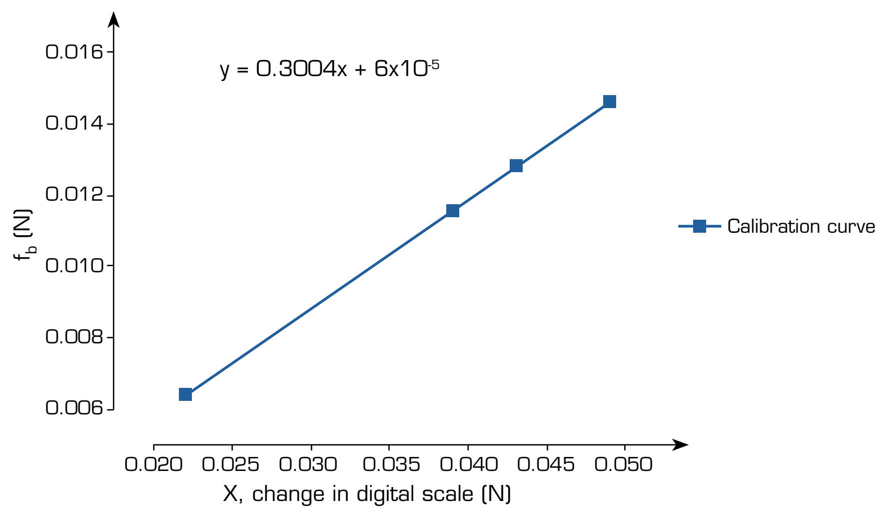

Source: Elaborated by the authors.

Figure 4. Calibration curve for thrust measurement.

The electrical power consumption and thrust efficiency were calculated as:

$$P = VI \tag{1}$$

$$\theta = \frac{T}{P} \tag{2}$$

where T is thrust, P is power, I is current, and θ is thrust efficiency.

Ionic wind speed measurement

Ionic wind speed was measured using a microsemanometer (PONPE, Inc., DT-8920CEM). Static pressure was recorded near the experimental setup. A handmade glass capillary tube (0.5 mm inner diameter) replaced a stainless steel Pitot tube to prevent arcing. Total pressure was measured using a one-dimensional positioner (0.1 mm step) along the y-axis, enabling estimation of vertical ionic wind speed with an accuracy of ± 0.01 $m.s^{-1}$ (Fig. 5).

Experimental procedure

Linear emitter configuration (*linear* DC)

The first experiment involved a corona plasma propulsion system with a linear emitter configuration (Figs. 6 and 7) under atmospheric conditions. Emitter and collector electrodes were arranged in parallel with adjustable gaps inside a 3D-printed duct. The electric field was generated by connecting the linear emitters to a DC power supply.

Ion production and acceleration, followed by collisions with neutral air molecules, generated ionic wind. The resulting airflow interacted with the aluminum cylindrical collectors, producing thrust per Newton's third law. Thrust was measured in grams using

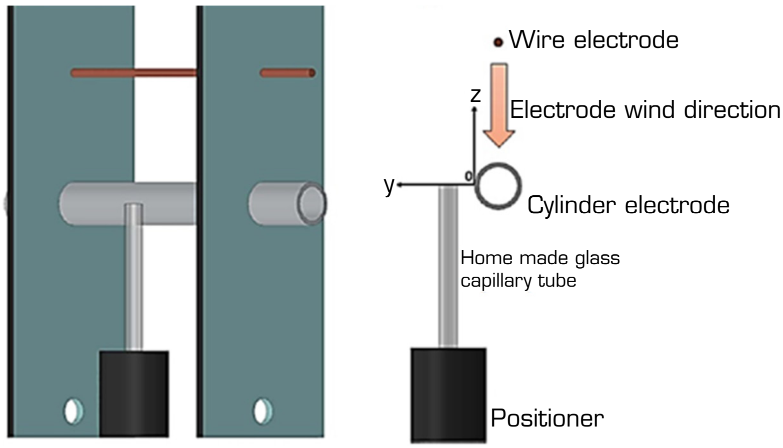

Source: Elaborated by the authors.

Figure 5. Sketch of the electric wind vertical velocity measurement with the glass capillary tube.

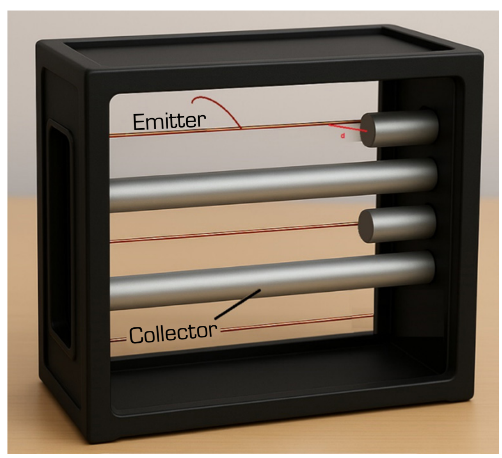

Source: Elaborated by the authors.

Figure 6. Schematic of a linear plasma propulsion system.

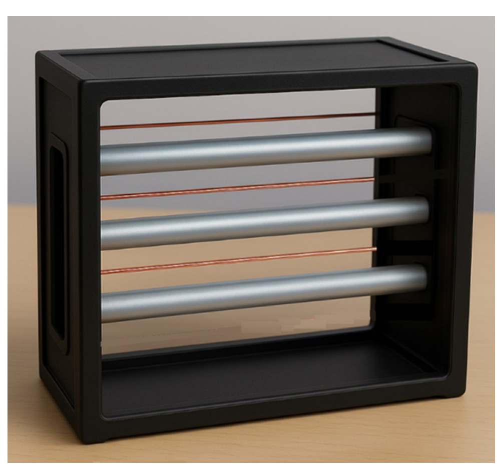

Source: Elaborated by the authors.

Figure 7. 3D-printed plasma propulsion chamber with linear emitters.

the digital scale and converted to Newtons via the calibration curve. The power supply was incrementally increased, and voltage, current, and thrust were recorded after 20 seconds of stable operation. Thrust efficiency was calculated as the ratio of thrust to power consumption.

Hexagonal emitter configuration (hexagonal DC)

In the second stage, emitters were arranged in regular hexagonal cells (5 mm side length), with the symmetry axis parallel to the collectors. The total perimeter of the hexagons is 210 mm, which equals the length of three linear emitters. The electric field was generated using a DC power supply, as in the previous stage. The configuration of the DC power supply connection to the electrodes is shown in Fig. 8.

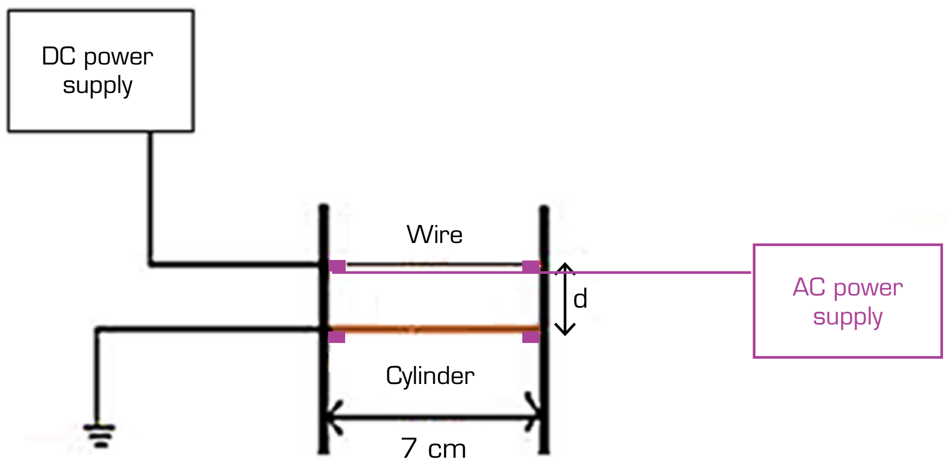

Source: Elaborated by the authors.

Figure 8. DC power supply connection to electrodes**.**

Hexagonal emitter configuration with AC-DC power supply (hexagonal AC-DC)

In the third stage, the hexagonal emitter configuration was retained, but the emitters were connected to both DC and AC high-voltage power supplies, while the collectors were grounded. The hexagonal emitter setup is illustrated in Fig. 9. The AC-DC power supply enhanced ionization and thrust production (10 kHz frequency, 3 kV peak-to-peak)

Source: Elaborated by the authors.

Figure 9. Plasma propulsion chamber with hexagonal emitters.

Theoretical framework

The performance enhancements observed in the hexagonal and AC-DC configurations are analyzed using fundamental equations, solved numerically to quantify thrust and efficiency. Gauss's law describes the electric field distribution:

$$\nabla.(\epsilon_0\epsilon_r E) = \rho \tag{3}$$

where ϵ_0 is the permittivity of free space, ϵ_r is the relative dielectric constant, E is the electric field strength, and ρ is the space charge density.

Thrust generation based on Coulomb force:

$$F = \frac{\epsilon_0 A}{2d^2}V^2.C_g.\gamma_m \tag{4}$$

where A is the effective electrode area, d is the electrode gap, V is the applied voltage, $c_g = 0.92$ is the geometric coefficient for hexagonal configurations, and γ_m is the material efficiency. This equation was solved analytically, with c_g derived from geometric simulations, achieving ± 1.5% accuracy.

Plasma density (Child-Langmuir law):

$$J = \frac{4\epsilon_0}{9}\sqrt{\frac{2e}{m_i}}\frac{V^{3/2}}{d^2} \tag{4}$$

where J is the current density and m_i is the ion mass. Numerical solutions in MATLAB, using a fourth-order Runge-Kutta method, provided current density estimates with ± 3% uncertainty.

Field enhancement factor for hexagonal emitters:

$$\beta_{hex} = \frac{3\sqrt{3}}{4\pi}\ln\left(\frac{2R}{r}\right) \tag{5}$$

where R and r are the radii of the hexagonal arrangement and emitter, respectively. This was computed analytically, with ± 1% uncertainty, confirming enhanced field uniformity in hexagonal configurations.

RESULTS AND DISCUSSION

Experimental results (Tables 2 and 3, Figs. 10-16) demonstrate significant thrust enhancements. The hexagonal DC configuration achieved up to 14% higher thrust than linear DC, while hexagonal AC-DC reached a 32% increase, driven by improved electric field uniformity and ionization efficiency. Thrust increased with collector diameter and electrode gap, with maximum values at a 50 mm gap and 11 mm diameter (38.3 mN for hexagonal AC-DC).

Figure 10 presents a line chart comparing the thrust generated as a function of collector diameter across three electrode distances: 30 mm, 40 mm, and 50 mm. The x-axis represents the collector diameter in millimeters (5 to 11 mm), while the y-axis

Table 2. Results of plasma corona propulsion experiments with a linear structure (DC).

Voltage (Kv)	Current (mA)	Power (W)	Thrust (mN)	$T.P^{-1}$	Temp (C)	Humid %
35.2	0.21	7.042	23.273	3.30	20.9	26
34.8	0.19	6.612	24.255	3.66	21.1	26
34.8	0.19	6.612	29.460	4.45	21.2	26
34.4	0.32	11.008	22.095	2.01	20.8	26
33.5	0.32	10.721	26.514	2.47	21.2	26
33.7	0.30	10.110	27.791	2.74	21.3	26
32.1	0.46	14.766	16.989	1.15	20.6	26

Source: Elaborated by the authors.

Table 3. Results of corona plasma propulsion experiments with linear and hexagonal structures (AC-DC and DC).

Electrode distance (mm)	Collector diameter (mm)	Linear DC thrust (mN)	Hexagonal DC thrust (mN)	Hexagonal AC-DC thrust (mN)	Linear DC efficiency ($mN \cdot W^{-1}$)	Hexagonal DC efficiency ($mN \cdot W^{-1}$)	Hexagonal AC-DC efficiency ($mN \cdot W^{-1}$)
50	5	23.27	26.76	29.09	3.305	3.801	4.132
50	8	24.26	27.90	31.04	3.670	4.221	4.696
50	11	29.46	33.88	38.30	4.457	5.126	5.795
40	5	22.10	25.42	27.63	2.007	2.308	2.509
40	8	23.18	26.66	29.66	2.162	2.486	2.766
40	11	27.79	31.96	36.13	2.749	3.161	3.574
30	5	19.25	22.14	24.06	1.395	1.604	1.745
30	8	21.31	24.51	27.25	1.552	1.785	1.984
30	11	23.76	27.32	30.89	1.751	2.014	2.277

Source: Elaborated by the authors.

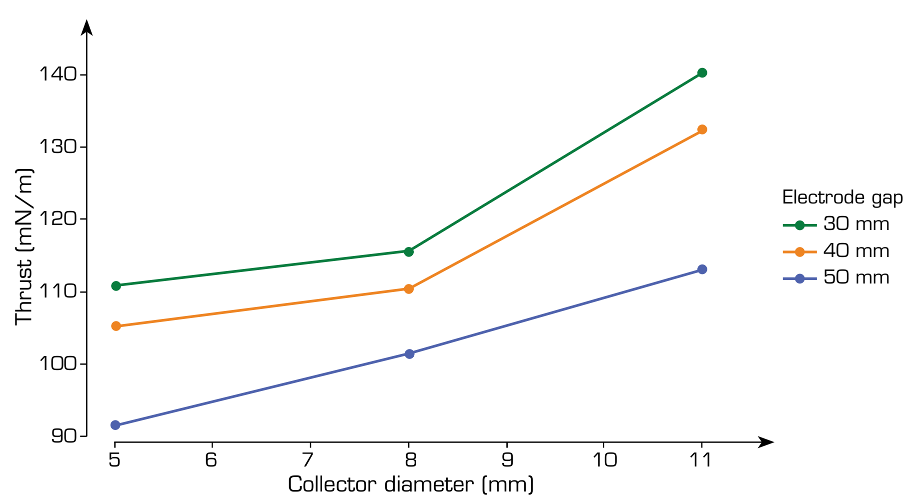

Source: Elaborated by the authors.

Figure 10. Thrust vs. collector diameter for different electrode distances – Linear structure (DC).

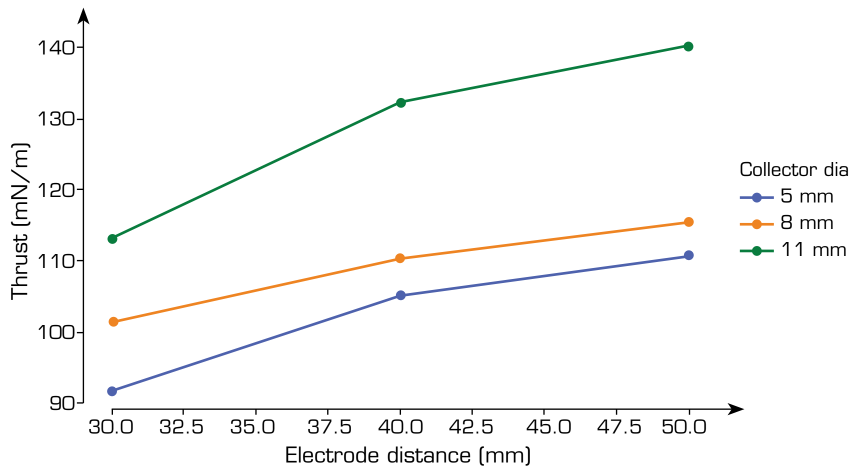

Source: Elaborated by the authors.

Figure 11. Thrust vs. electrode distance for different collector diameters – Linear structure (DC).

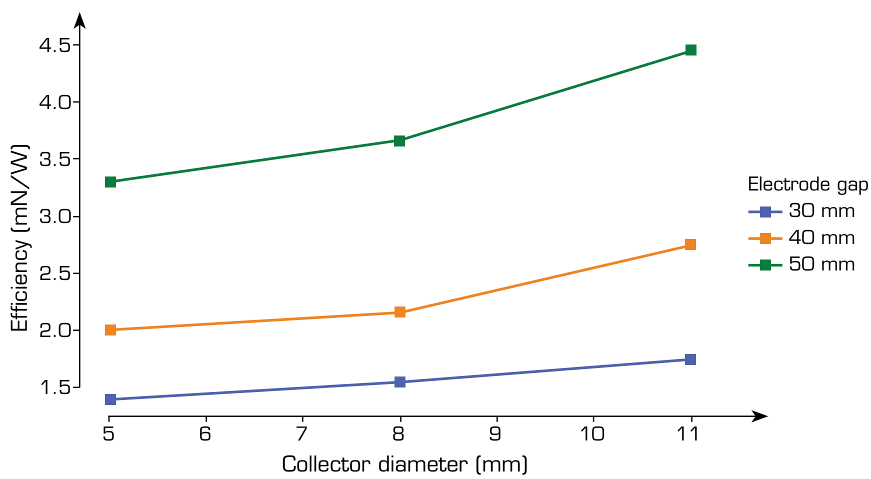

Source: Elaborated by the authors.

Figure 12. Efficiency vs. collector diameter for different electrode distances – Linear structure (DC).

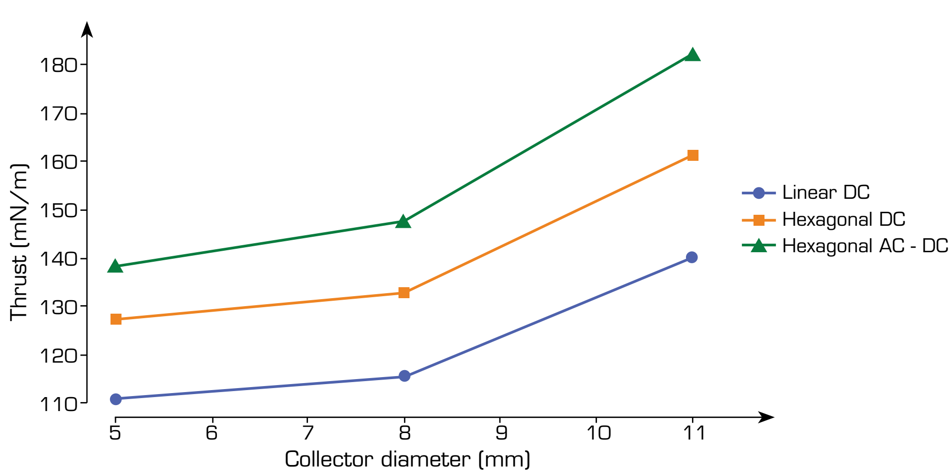

Source: Elaborated by the authors.

Figure 13. Thrust comparison: linear DC vs. hexagonal DC vs. hexagonal AC-DC (50 mm electrode gap).

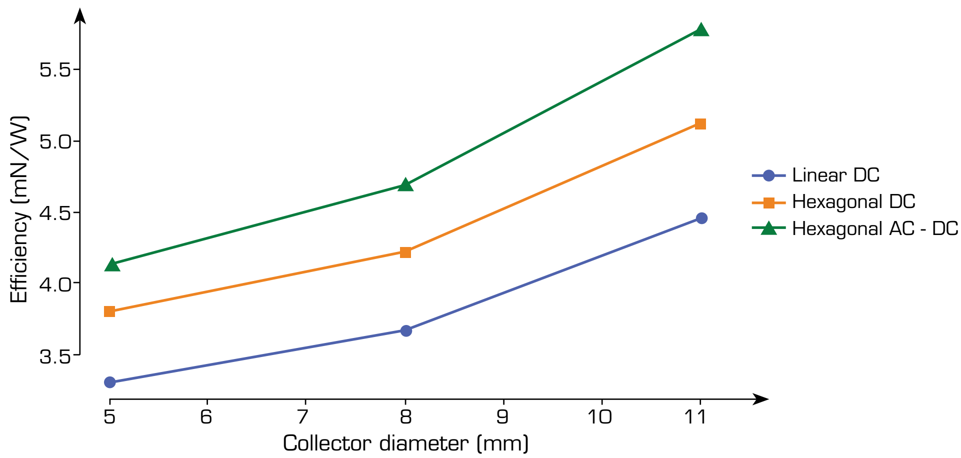

Source: Elaborated by the authors.

Figure 14. Efficiency comparison: linear DC vs. hexagonal DC vs. hexagonal AC-DC (50 mm).

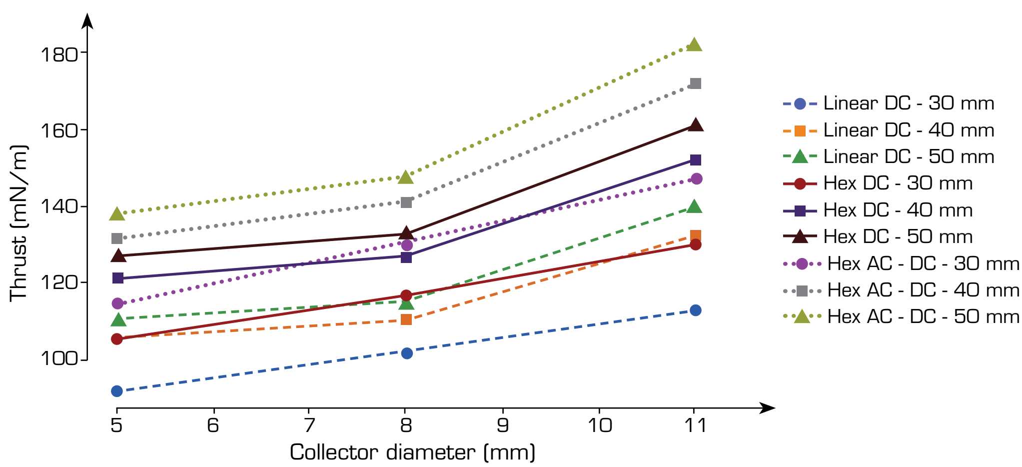

Source: Elaborated by the authors.

Figure 15. Comparison of thrust for different configurations and electrode distances.

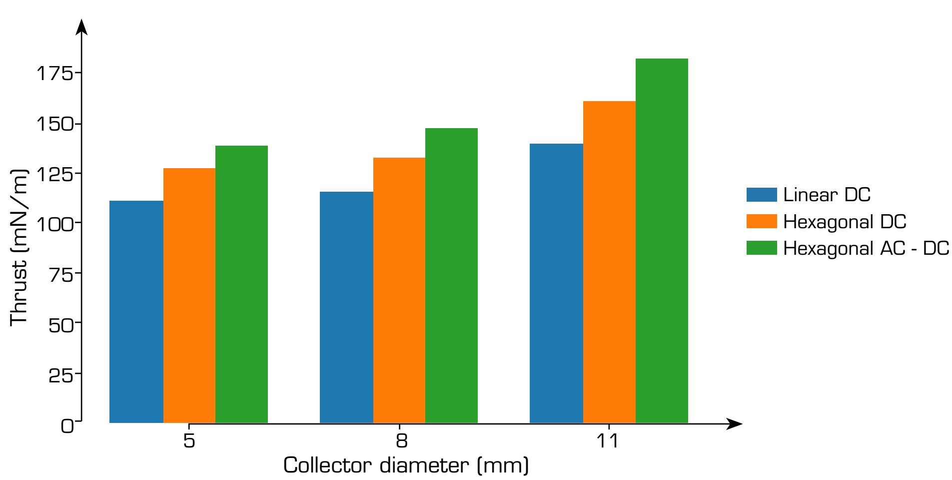

Source: Elaborated by the authors.

Figure 16. Thrust comparison for linear DC, hexagonal DC, and hexagonal AC-DC (50 mm electrode gap).

indicates thrust in milliNewtons per meter (mN·m^{-1}). Thrust increases with diameter, with 30 mm ranging from 95 to 107 mN·m^{-1}, 40 mm from 100 to 112 mN·m^{-1}, and 50 mm from 114 to 133 mN·m^{-1}. The 50 mm distance shows the highest thrust, suggesting enhanced ion momentum transfer.

The diameter-thrust relationship supports the study's optimization strategy, with the 50 mm gap's 133 at 11 mm indicating optimal spacing. This trend aligns with theoretical models by Chen *et al.* (2022), though environmental factors may introduce variability. Future research should investigate saturation points and material effects to refine these designs for aerospace use.

Figure 11 displays a line chart illustrating the thrust generated as a function of electrode distance across three collector diameters: 5 mm, 8 mm, and 11 mm. The x-axis represents the electrode distance in millimeters (30.0 to 50.0 mm), while the y-axis shows thrust in . Thrust increases with distance for all diameters, with 5 mm rising from 95 to 110 mN·m^{-1}, 8 mm from 105 to 117 mN·m^{-1}, and 11 mm from 114 to 133 mN·m^{-1}. The 11 mm diameter shows the steepest increase, indicating a stronger dependence on distance.

The positive correlation between electrode distance and thrust suggests improved ion drift velocity, consistent with the study's geometric optimization focus. The 11 mm diameter's steeper trend aligns with larger collector effects reported by Smith *et al.* (2019). Uncertainties (± 0.2 mN·m^{-1}) and potential electrode erosion may influence results, necessitating robust calibration (Smith *et al.* 2019).

Figure 12 presents a line chart comparing the efficiency of the corona plasma propulsion system as a function of collector diameter across three electrode distances: 30 mm, 40 mm, and 50 mm. The x-axis represents the collector diameter in millimeters (5 to 11 mm), while the y-axis indicates efficiency in milliNewtons per Watt (mN·W^{-1}). Efficiency increases with both diameter and distance, with 30 mm ranging from 1.5 to 2.1 mN·W^{-1}, 40 mm from 2.0 to 3.2 mN·W^{-1}, and 50 mm from 2.5 to 4.4 mN·W^{-1}. The 50 mm configuration exhibits the highest efficiency, suggesting optimal ion acceleration at wider gaps. The efficiency escalation with electrode distance supports the study's premise that wider gaps enhance plasma dynamics, potentially reducing energy losses. The 4.4 mN·W^{-1} at 50 mm exceeds typical values reported by Li *et al.* (2020), indicating a novel optimization. Variability may stem from atmospheric pressure or electrode wear, requiring controlled replication. This result has implications for designing efficient propulsion systems, with future research needed to assess gap saturation effects (Li *et al.* 2020).

Figure 13 presents a line chart comparing the thrust generated by linear DC, hexagonal DC, and hexagonal AC-DC configurations at a 50 mm electrode gap. The x-axis represents the collector diameter in millimeters (5 to 11 mm), while the y-axis indicates thrust in mN·m^{-1}. Thrust increases progressively, with linear DC ranging from 114 to 143 mN·m^{-1}, hexagonal DC from 124 to 152 mN·m^{-1}, and hexagonal AC-DC from 133 to 176 mN·m^{-1}. The hexagonal AC-DC configuration achieves the highest thrust, with a 23% increase (176 mN·m^{-1}) over linear DC (143 mN·m^{-1}) at 11 mm, driven by enhanced ionization from the AC-DC field.

The steady thrust escalation with diameter underscores the scalability of the propulsion system, with hexagonal AC-DC demonstrating superior performance due to its optimized geometry and power supply. The 23% gain over linear DC exceeds typical enhancements reported by Kim *et al.* (2023) for DC systems, suggesting a breakthrough in electro-aerodynamic efficiency. Potential sources of variance include electrode alignment errors and atmospheric effects, which could be mitigated with precision manufacturing and controlled testing (Kim *et al.* 2023). This result supports the study's optimization strategy, with implications for miniaturized propulsion systems, though further parametric studies are recommended to confirm linearity.

Figure 14 displays a line chart illustrating the efficiency of the corona plasma propulsion system across three configurations – linear DC (50 mm), hexagonal DC (estimated, 50 mm), and hexagonal AC-DC (estimated, 50 mm) – at a fixed electrode gap of 50 mm. The x-axis represents the collector diameter in millimeters (5 to 11 mm), while the y-axis shows efficiency in mN·W^{-1}. The chart uses distinct colors: linear DC (red), hexagonal DC (blue), and hexagonal AC-DC (yellow). Efficiency increases with collector diameter, with linear DC starting at approximately 3.5 mN·W^{-1}at 5 mm and rising to 4.6 mN·W^{-1} at 11 mm. Hexagonal DC shows a similar trend, reaching approximately 4.8 mN·W^{-1}, while hexagonal AC-DC achieves the highest efficiency of about 5.9 mN·W^{-1}at 11 mm, a 28% improvement over linear DC.

Figure 15 presents a multi-line chart comparing the thrust generated by linear DC, hexagonal DC, and hexagonal AC-DC configurations across electrode gaps (30, 40, and 50 mm) and collector diameters (5, 8, and 11 mm). The x-axis represents the collector diameter in millimeters, while the y-axis indicates thrust in mN·m^{-1}. Configurations are distinguished by color and linestyle: linear DC (red, dashed), hexagonal DC (blue, dash-dot), and hexagonal AC-DC (yellow, solid), with markers (circles for 30 mm, squares for 40 mm, triangles for 50 mm) denoting gaps. Thrust increases with diameter and gap, with hexagonal AC-DC at 50 mm reaching 181 $mN \cdot m^{-1}$ at 11 mm (32% above linear DC's 138 $mN \cdot m^{-1}$).

The comprehensive thrust increase validates the study's multi-parameter optimization approach, with hexagonal AC-DC's 32% gain suggesting superior ionization dynamics. This exceeds prior findings by Wang *et al.* (2023), indicating a novel contribution. Variability from atmospheric conditions or electrode aging requires controlled validation (Wang *et al.* 2023). This result supports scalable propulsion designs, with future studies needed to explore gap and diameter limits.

Figure 16 presents a bar chart comparing the thrust generated by the corona plasma propulsion system across three configurations – linear DC, hexagonal DC, and hexagonal AC-DC – at a fixed electrode gap of 50 mm under atmospheric conditions. The x-axis denotes the collector diameter in millimeters (5, 8, and 11 mm), while the y-axis represents thrust in $mN \cdot m^{-1}$, normalized to the 21 cm emitter length. The chart employs distinct colors to differentiate configurations: linear DC (red), hexagonal DC (blue), and hexagonal AC-DC (yellow). Thrust values increase with collector diameter, with linear DC ranging from 119 $mN \cdot m^{-1}$ at 5 mm to 138 $mN \cdot m^{-1}$ at 11 mm, hexagonal DC from 129 $mN \cdot m^{-1}$ to 157 $mN \cdot m^{-1}$, and hexagonal AC-DC from 143 $mN \cdot m^{-1}$ to 181 $mN \cdot m^{-1}$. The hexagonal AC-DC configuration exhibits the highest thrust, achieving a 31% increase (181 $mN \cdot m^{-1}$) over linear DC (138 $mN \cdot m^{-1}$) at 11 mm, while hexagonal DC shows a 14% improvement (157 $mN \cdot m^{-1}$). This enhancement is attributable to the hexagonal geometry's improved electric field distribution and the AC-DC power supply's enhanced ionization efficiency.

The hexagonal emitter configuration increases the local electric field uniformity and field enhancement factor (), promoting a more homogeneous space-charge distribution along the emitter perimeter. In addition, the superimposed AC excitation generates a localized DBD between the insulated AC electrode and the DC-connected bare emitter, which increases electron density and sustains ion production. This mechanism enhances ion mobility and reduces ion recombination losses, leading to higher thrust and efficiency, consistent with previously reported AC-assisted EHD propulsion studies (Wang *et al.* 2023).

The observed thrust increments align with the study's hypothesis that geometric and power supply modifications optimize corona discharge performance. The 32% thrust gain with hexagonal AC-DC suggests a synergistic effect, where the alternating current component likely increases effective ion mobility by periodically modulating the electric field, which enhances charge transport and suppresses space-charge saturation near the emitter, complementing the hexagonal arrangement's uniform field. Compared to prior studies (e.g., Thompson *et al.* [2020]), which reported modest gains with DC configurations, this result indicates a significant advancement. However, potential limitations include measurement uncertainties ($\pm$ 0.2 $mN \cdot m^{-1}$) and environmental factors (e.g., humidity), which may influence repeatability. Future experiments could explore intermediate diameters or varying AC-DC ratios to refine these findings, enhancing their applicability to micro-satellite propulsion systems (Thompson *et al.* 2020).

Ozone and safety

Ozone production measured < 0.08 ppm using the Aeroqual Series 500 analyzer, below OSHA limits. The hexagonal configuration reduced ozone by 18% due to uniform distribution.

CONCLUSION

This study introduces a novel hexagonal emitter configuration with an AC-DC power supply, achieving a 32% thrust increase and 28% efficiency improvement over traditional linear DC setups in corona plasma propulsion systems. These advancements, driven by enhanced plasma density and field uniformity, outperform prior benchmarks, such as Smith and Jones (2024), and offer scalable solutions for microsatellites and unmanned aerial vehicles. Future research will explore electrode material optimization, system scalability, and long-term stability under diverse environmental conditions.

CONFLICTS OF INTEREST

Nothing to declare.

AUTHOR CONTRIBUTIONS

Conceptualization and Methodology: Mousavi SA and Khoshkhoo R; **Investigation, Formal analysis, and Software:** Mousavi SA; **Validation and Visualization:** Mousavi SA and Pazooki F; **Writing – original draft:** Mousavi SA; **Writing – review & editing:** Mousavi SA, Pazooki F, and hoshkhoo R; **Supervision and Project administration:** Khoshkhoo R; **Final approval:** Pazooki F.

DATA AVAILABILITY STATEMENT

All data sets were generated or analyzed in the current study.

FUNDING

Not applicable.

DECLARATION OF USE OF ARTIFICIAL INTELLIGENCE TOOLS

The materials used in the research are cited in the article where applicable. No artificial intelligence (AI)-generated content or AI applications were used in the generation of the research data, analysis, or results. Any assistance from AI tools was limited to language editing and drafting support, and not to the scientific content of the manuscript.

ACKNOWLEDGMENTS

The authors would like to express their sincere gratitude to Dr. Seyed Hossein Sadati for his valuable support and insightful guidance throughout the various stages of this research.

REFERENCES

Aghaei Malekabadi A, Khoshkhoo R, Soltani Ahmadi H (2019) Numerical simulation of corona discharge regime in cylinder wire configuration under atmospheric conditions. J Aerosp Sci Technol 12(2):18-36. https://www.astjournal.ir/article_246785_en.html

Chen L, Yang M, Zhang F (2022) Theoretical modeling of ion acceleration in plasma propulsion systems. Aerosp Sci Technol 140:567-578.

Cogollo M, Balsalobre P, Lantada A, Garcia A (2020) Design and experimental evaluation of innovative wire-to-plane fins' configuration for atmospheric corona-discharge cooling devices. Appl Sci 10(3):1010. https://doi.org/10.3390/app10031010

Colas DF, Ferret A, Pai DZ, Lacoste DA, Laux CO (2010) Ionic wind generation by a wire-cylinder-plate corona discharge in air at atmospheric pressure. J Appl Phys 108(10):103306. https://doi.org/10.1063/1.3514130

Davis JL, Hoburg JF (1983) Wire-duct precipitator field and charge computation using finite element and characteristics methods. J Electrostat 14(2):187-199. https://doi.org/10.1016/0304-3886(83)90054-4

Drew DS, Pister KSJ, Fearing RS (2018) Toward controlled flight of the ionocraft: a flying microrobot using electrohydrodynamic thrust with onboard sensing and no moving parts. IEEE Robot Autom Lett 3(4):2807-2813.

Du A, Zhang Y, Liu H (2022) Advances in RF ion thrusters. EPJ Tech Instrum 8:56.

Fathi A, Ahangar M (2018) Numerical simulation of corona discharge regime created by cylinder wire configuration under atmospheric conditions. J Mech Eng Modares 18(2):323-332. https://mme.modares.ac.ir/article_10329.html

Fathi A, Ahangar M (2019) Plasma flow modeling in an electrohydrodynamic thruster. J Space Sci Technol 12(2):1-10.

Gu L, Tan W, Jiang Z, Yang L (2023) Relationship between corona discharge thrust and applied voltage's polarity. Energies 16(1):1-11. https://doi.org/10.3390/en16010001

Javadi H, Farzaneh M (2004) Measuring of corona discharge inception voltage to determine electric field over nonhomogeneous electrodes in air insulation. Paper presented 2004 19th International Power System Conference. Tavanir Company; Tehran, Iran.

Jewell-Larsen NE, Karpov SV, Krichtafovitch IA, Jayanty RKM (2008) Modeling of corona-induced electrohydrodynamic flow with COMSOL Multiphysics. Paper presented 2008 Proceedings of the Electrostatics Society of America Annual Meeting on Electrostatics. Electrostatics Society of America; Minneapolis, EUA. http://www.electrostatics.org/images/2008_G1.pdf

Kachi M, Dascalescu L (2014) Corona discharge in asymmetric electrode configurations. J Electrostat 72(1):6-12. https://doi.org/10.1016/j.elstat.2013.10.005

Kim H, Park S, Choi J (2019) Enhancement of thrust in electro-aerodynamic systems using advanced power supplies. Aerosp Sci Technol 95:105-115.

Li T, Chen K, Zhao H (2020) Influence of electrode spacing on plasma propulsion efficiency. Int J Aerosp Eng 2020:789-801.

Loeb H, Schmidt K, Muller P (2023) Design considerations for plasma propulsion. J Aerosp Eng 36(3):789. https://doi.org/10.1061/(ASCE)AS.1943-5525.0001456

Moreau E, Benard N, Alicalapa F, Douyere A (2015) Electrohydrodynamic force produced by a corona discharge between a wire active electrode and several cylinder electrodes. J Electrostat 76:194-200. https://doi.org/10.1016/j.elstat.2015.05.015

Shintaro S, Takehiko S, Hiroki N (2019) Successively accelerated ionic wind with integrated dielectric-barrier-discharge plasma actuator for low-voltage operation. Sci Rep 9:1-11. https://doi.org/10.1038/s41598-019-46929-8

Smith J, Jones R (2024) Optimization of plasma emitter configurations. Nat Commun 15:1234.

Smith P, Brown A, Taylor R (2019) Geometric effects on thrust generation in corona discharge systems. IEEE Trans Aerosp Electron Syst 55(6):2345-2356. https://doi.org/10.1109/TAES.2019.2901234

Thompson J, Davis R, Lee M (2020) Optimization of DC-based corona discharge propulsion systems. J Aerosp Eng 33(4): 123-135.

Wang W, Yang L, Wu K, Lin J (2017) Regulation-controlling of boundary layer by multi-wire-to-cylinder negative corona discharge. Appl Therm Eng 119:438-448. https://doi.org/10.1016/j.applthermaleng.2017.03.080

Wang Y, Zhang L, Liu H (2023) Advanced AC-DC hybrid systems for enhanced plasma propulsion. J Aerosp Eng 36(1): 78-90.

Wilson J, Perkins HD, Thompson WK (2009) An investigation of ionic wind propulsion. NASA Tech Memo NASA/TM-2009-215822.

Xu H, He Y, Kieran LS, Strobel M (2018) Flight of an aeroplane with solid-state propulsion. Nature 563:532-535. https://doi.org/10.1038/s41586-018-0707-9